Multi-Channel Facial Photoplethysmography Sensing

Parker S. Ruth*, Jerry Cao, Millicent Li, Jacob E. Sunshine, Edward J. Wang, Shwetak N. Patel

***Abstract*— Motivated by the need for continuous cardiovascular monitoring, we present a system for performing photoplethysmography sensing at multiple facial locations. As a proof-of-concept, our system incorporates an optical sensor array into a wearable face mask form factor for application in a surgical hemodynamic monitoring use case. Here we demonstrate that our design can accurately detect pulse timing by validating estimated heart rate against ground truth electrocardiogram recordings. In an experiment across 10 experimental subjects, our system achieves an error standard deviation of 2.84 beats per minute. This system shows promise for performing non-invasive, continuous pulse waveform recording from multiple locations on the face.**

I. Introduction

Non-invasive pulse waveforms encode essential information about the cardiovascular system. Photoplethysmography (PPG) enables continuous measurement of pulse waveforms using non-invasive optical sensors. Timing and information extracted from PPG waveforms can be used to compute a multitude of informative vital signs, including heart rate, heart rate variability, respiratory rate, and cardiac output. Measuring pulse timing at multiple locations enables the estimation of arterial stiffness and blood pressure from the traversal of pulse waveforms throughout the vasculature. Although existing PPG sensing technologies record from the finger (e.g. surgical pulse oximeters) or wrist (e.g. smart watches), the face presents a promising and underutilized location for wearable pulse sensing.

As a proof-of-concept, we demonstrate a potential application of our facial PPG sensing system for a surgical use case. Since brief intervals of low blood pressure can result in serious adverse patient outcomes, including acute kidney injury, myocardial injury, stroke, and death [1], [2], it is an anesthetic management standard of care to measure blood pressure during every surgery [3], [4]. However, among the 20 million surgeries performed annually in the United States [5], the vast majority use oscillometric blood pressure cuffs, which provide readings on 3-5 minute intervals that are too infrequent to detect rapid blood pressure changes. While intra-arterial catheters enable beat-to-beat pulse waveform monitoring, the risks associated with their invasiveness preclude their routine use [6]. Since facial PPG signals have been shown to enable non-invasive blood pressure estimation using pulse transit time between facial arteries [7], our facial PPG sensing system has the potential to be applied to continuous anesthetic blood pressure management.

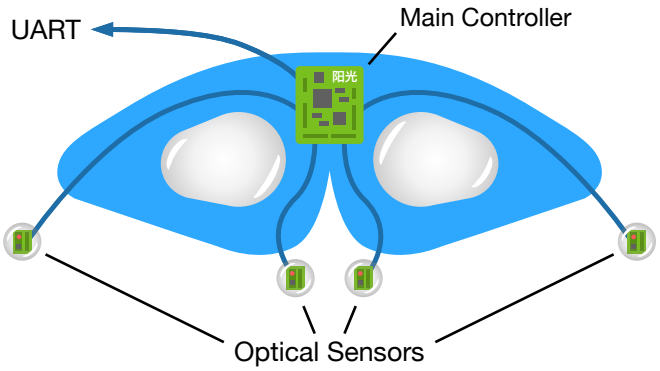

Fig. 1. Illustration of face mask with integrated optical sensing system

In this work, we demonstrate the incorporation of our sensing system with a surgical eye protection face mask, which is used in surgeries to minimize risk of corneal abrasion [8], [9]. By enabling continuous pulse waveform recordings without the need for an invasive procedure, this application of our system could improve intraoperative hemodynamic monitoring. To evaluate the accuracy of pulse timing measured by our device, we validated the beat-to-beat heart rate computed from our facial pulse sensors against ground truth electrocardiogram heart rate.

II. Methods

A. Face Mask Hardware Design

The device hardware consists of an electronic system that can be attached to a disposable Dupaco Opti-Gard$^{\hat{A}®}$ face mask backing (Fig. 1). The circuit is composed of a central controller with four peripheral sensing modules (Fig. 2). The main controller module consists of an MSP430 FR2355 microprocessor (Texas Instruments) which communicates over an I2C bus with an ADPD 1080 analog front-end (Analog Devices). The analog front-end drives the optical sensor modules, which are implemented with the SFH 7072 multi-chip package (Osram). Power and data transfer are provided

*Corresponding author
Parker S. Ruth is with the Paul G. Allen School of Computer Science & Engineering and the Department of Bioengineering, University of Washington, Seattle, WA 98195, USA. E-mail: psr23@cs.washington.edu
Jerry Cao and Millicent Li are with the Paul G. Allen School of Computer Science & Engineering, University of Washington, Seattle, WA 98195, USA. E-mails: {jcao22, limill01}@cs.washington.edu
Jacob E. Sunshine is with the Department of Anesthesiology & Pain Medicine, University of Washington, Seattle, WA 98195, USA. E-mail: jesun@uw.edu
Edward J. Wang is with the Department of Electrical and Computer Engineering and the Design Lab, University of California, San Diego, CA 92093, USA. E-mail: ejaywang@eng.ucsd.edu
Shwetak N. Patel is with the Paul G. Allen School of Computer Science & Engineering and the Department of Electrical & Computer Engineering, University of Washington, Seattle WA 98195, USA. E-mail: shwetak@cs.washington.edu

978-1-7281-1990-8/20/$31.00 ©2020 IEEE

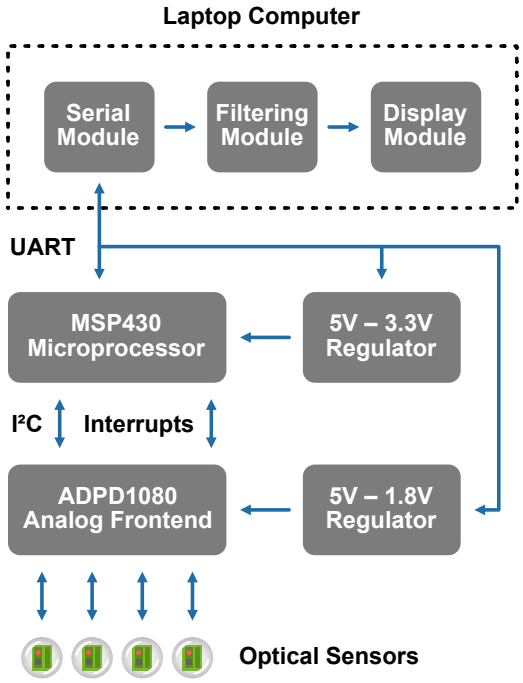

Fig. 2. Schematic of hardware and real time software modules.

through a physical 115200 baud rate UART connection to a data collection laptop.

The four optical sensors each record at two wavelengths for a total of 8 channels. Each optical sensor module is fully encapsulated in a coat of Dragon Skin™ 10 Very Fast silicone rubber to prevent electronic components from directly contacting skin. To avoid interfering with optical measurements, the silicone rubber is less than 1 mm over the LEDs and photodiodes. A custom mold was designed to maintain consistent silicone thickness across all sensors.

B. Optoelectronics

Each optical sensor module is configured to record optical reflectance at red and infrared (IR) wavelengths, with peak emissions at 660 nm and 950 nm respectively. The analog frontend is configured to supply the red and IR light emitting diodes (LEDs) with 250 mA current, and reflected light is measured by a broadband photodiode. To reduce noise, each sample is averaged over 128 sequential 2 µs pulses, with 25 µs delay between the red and IR LED pulse trains.

The face mask samples all eight channels at a frequency of 141 Hz. Each sample is serially encoded as a string of 32 bytes of data (four bytes per channel) followed by a single byte delimiter for channel alignment. The laptop runs an in-house Python script to record the raw bytes from the face mask, apply real time IIR filters, and display the output to the user for visualization (Fig. 2).

C. Experimental Setup

We recruited n = 10 subjects to participate in a validation study. Participants wore the face mask with sensors taped over the superficial temporal arteries (near the temple) and

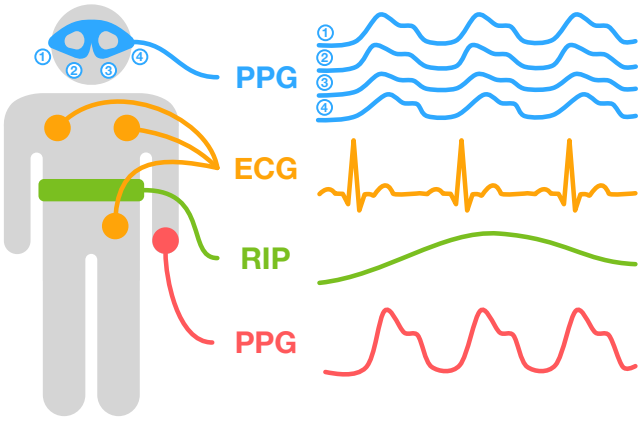

Fig. 3. Schematic of experimental setup and recording channels.

angular arteries (near the nose); these measurement locations were informed by prior work [7]. Pulse waveforms were recorded from the optical sensors, and ground truth vital signs were simultaneously recorded with a BioRadio wireless physiological monitor from Great Lakes Neurotechnologies (Fig. 3). The BioRadio recorded electrocardiography (ECG) from three-lead gel electrodes (1000 Hz), respiratory inductance plethysmography (RIP) from an elastic chest strap (1000 Hz), and photoplethysmography (PPG) from the left index finger (83 Hz).

To induce variation in heart rate and blood pressure, subjects were instructed to alternate between breathing normally and holding their breath at full inhalation capacity for periods of 20 seconds (Table I). Subjects were seated during all measurements. The experimental protocol was approved by an institutional review board with written consent obtained from all participants.

TABLE I
EXPERIMENTAL PROCEDURE

State	Activity	Duration
1	resting	60 seconds
2	holding breath	20 seconds
3	resting	60 seconds
4	holding breath	20 seconds
5	resting	60 seconds
6	holding breath	20 seconds
7	resting	60 seconds

D. Signal Processing and Analysis

The facial PPG signal was processed with the following filters:

1) Chebyshev Type II lowpass IIR filter (6th order, 7 Hz cutoff, 2 dB ripple, 100 dB stop band attenuation).
2) Baseline removal with 1-second Hamming window.[1]
3) Chebyshev Type II highpass IIR filter (3rd order, 0.15 Hz cutoff, 2 dB ripple limit, 40 dB stop band attenuation).

[1]Baseline removal was performed before highpass filtering to reduce edge effects from the IIR filter

Filters were implemented in Python using the SciPy library's `iirfilter` function. Filters were applied unidirectionally to the raw channel input. We chose to use Chebyshev Type II inputs, since they have been shown to perform well on PPG waveforms [10]. Filter parameters were chosen to accentuate peaks, reduce electrical noise, and preserve pulse waveform morphology across the full range of heart rates.

Regions of the pulse waveforms within the time window 2 seconds before and after a transition between states (Table I) were excluded from HR calculations due to motion artifacts.

The heart rate was computed from a linear combination of all eight sensor channels. For each subject, the clarity of the signal in each channel y_i was estimated by computing the power spectral density (PSD) of the N raw signal values (1), and taking the negative entropy within the range from 0.8 Hz to 1.8 Hz (2). The weights for all eight channels were taken as the normalized negative entropies (3), and the aggregated facial PPG signal was computed as a weighted sum of individual channels (4).

$$\mathrm{PSD}_i(f) = \frac{1}{N} \left| \mathcal{F}\left[y_i(t)\right](f) \right|^2 \tag{1}$$

$$e_i = \sum_{f=0.8}^{1.8} \mathrm{PSD}_i(f) \ln\left[\mathrm{PSD}_i(f)\right] \tag{2}$$

$$\mathbf{w} = \frac{\langle e_1, e_2, \ldots, e_8 \rangle^{\mathrm{T}} - \min(e_i)}{\max(e_i) - \min(e_i)} \tag{3}$$

$$\mathbf{y}^* = \langle y_1(t), y_2(t), \ldots, y_8(t) \rangle \cdot \mathbf{w} \tag{4}$$

Power spectral density was computed from only the first 10 seconds of the each recording. Peaks in all pulse waveform types were selected with a minimum peak-to-peak separation of 0.4 seconds and minimum peak height set by a dynamic threshold; the threshold at each time step was set from the local mean and standard deviation within a local 2-second Hamming window. Instantaneous heart rate was calculated as the difference between sequential pulse times. Instantaneous heart rate estimates were excluded if they fell below 40 BPM or above 120 BPM. Remaining outliers were removed by discarding points of with high second derivatives of the heart rate trend over time. Pulses detected from the face mask and ECG were paired if they occurred between 0.4 and 1 seconds of each other.

III. Results and Discussion

A. Signal Processing

Fig. 4 shows the facial PPG waveforms from the first 5 seconds of Subject 1 across all eight channels. It is typical for each location to exhibit pulsatility in a single wavelength. Since red and IR wavelengths penetrate the tissue at different depths, the location of the sensor relative to the artery determines the wavelength with the clearest signal. On Subject 1, the red wavelength dominates at the left temporal arterial measurement location, while infrared wavelengths are preferred at the other three locations; the distribution differs from subject to subject.

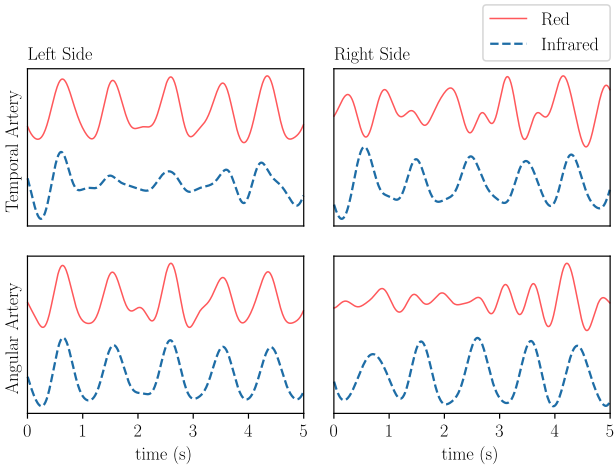

Fig. 4. Example facial PPG waveforms from eight channels on Subject 1.

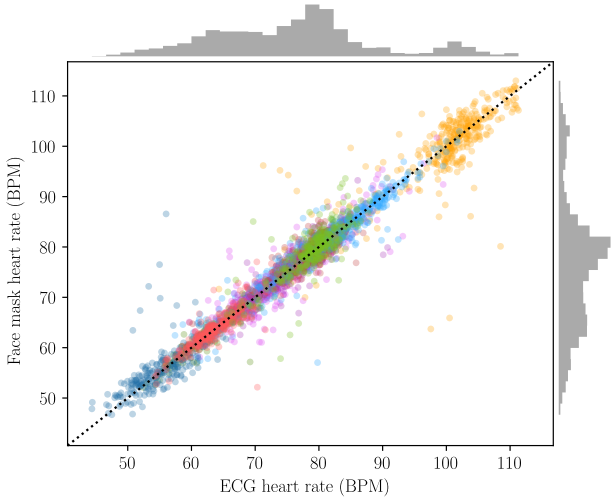

Fig. 5. Heart rate estimation correlation; colors represent different subjects

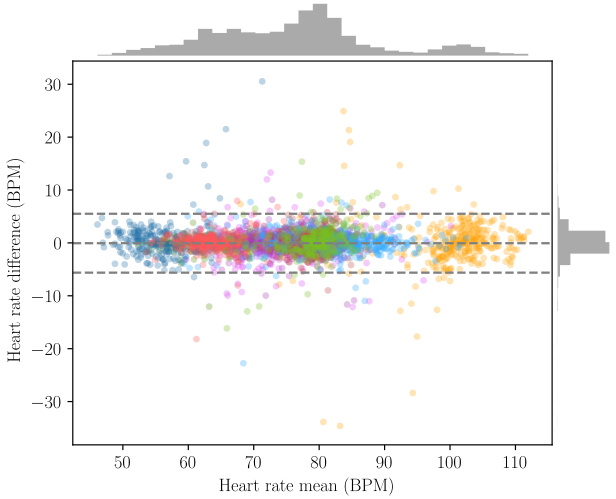

Fig. 6. Bland-Altman plot of HR error; colors represent different subjects

B. Heart Rate Estimation Accuracy

The correlation between heart rate estimated from facial PPG against ground truth ECG heart rate is shown in Fig. 5. Though most pulses are closely correlated (overall root mean squared error RMSE $= 2.84$, standard deviation of error 2.84, and coefficient of correlation $R = 0.975$), occasional outliers are present. These outliers are primarily caused by regions of high noise in the facial PPG waveforms due to movement artifacts from the subjects (e.g. blinking and swallowing) which would not be present in an anesthetized setting. The Bland-Altman plot of the HR estimation error (Fig. 6) illustrates close agreement with ground truth, with an overall error standard deviation of 2.84 BPM, which is not meaningful clinically. Full descriptive statistics for the HR error across subjects are shown in Table II. Across all 10 subjects, an average of 90% of beats were correctly detected by this algorithm (minimum 75%, and maximum 99%).

TABLE II
FACEMASK-DERIVED HR DESCRIPTIVE STATISTICS (BPM)

Subject	HR Mean	HR Std.	RMSE	Error Std.	R
1	65.26	5.99	1.34	1.34	0.975
2	74.82	5.91	2.24	2.24	0.930
3	99.07	8.54	4.98	4.97	0.828
4	74.53	8.01	3.31	3.31	0.912
5	76.19	5.26	2.11	2.11	0.917
6	77.24	6.15	1.90	1.90	0.952
7	55.66	5.04	4.07	4.01	0.635
8	82.88	7.45	1.85	1.85	0.970
9	63.99	4.13	1.91	1.91	0.893
10	79.28	4.70	2.83	2.81	0.800
All	76.14	12.74	2.84	2.84	0.975

C. Real Time Computation

Since waveforms were processed unidirectionally with IIR filters and convolutions, the signal conditioning can all be implemented in real time. Although the power spectrum density calculation is not a real-time computation, it was computed over only the first 10 seconds of data, which would enable the system to output results after an initial 10-second calibration interval.

D. Limitations and Future Work

Sources of noise in this prototype can primarily be attributed to sensor placement, power line noise, and analog signal attenuation along connecting wires. Since the device receives power from a laptop, poor grounding can impact the sensor fidelity; this can be improved by using an optical isolator and battery power supply, or with improved grounding.

A remaining limitation of this design is that it requires manual fixation of the optical sensors with medical tape; while tape is routinely applied to the face during surgery, future iterations should incorporate the sensors directly into the face mask substrate to improve the ease of usage and reduce sensor misplacement error. Future work should also test the usage of this device in the context of other surgical equipment and environmental factors.

The validation presented here examines only heart rate detection. Further characterization of the distribution of pulse timing at different facial locations is required to validate the potential for this design to be used for additional cardiovascular metrics such as arterial stiffness and blood pressure.

IV. CONCLUSION

We presented a novel system for recording facial photoplethysmogram measurements from multiple wavelengths and locations on the face. Our system is integrated with a surgical eye protection face mask, making it suitable for intraoperative hemodynamic monitoring. Our hardware device and software signal processing pipeline can perform accurate pulse detection, enabling beat-to-beat heart rate measurement that correlates well with ground truth electrocardiography measurements. Multiple measurement wavelengths enable robustness against sensor placement. This device shows promise for future applications in non-invasive, continuous monitoring of cardiac vital signs. More broadly, this work may have applications in other wearable form factors such as eyeglasses, protective headgear, and mixed reality headsets.

ACKNOWLEDGMENT

This research is supported by the Mary Gates Endowment for Students and the Levinson Emerging Scholars Program. P. S. R. wishes to thank Manuja Sharma for her thoughtful advice on optoelectronics SNR optimization, and Dr. Patrick Boyle for his thoughtful feedback on this manuscript. P. S. R. also wishes to thank his family for their outstanding support.

REFERENCES

[1] M. Walsh, A. Kurz, and L. Thabane, "Relationship between Intraoperative Mean Arterial Pressure and Clinical Outcomes after Noncardiac Surgery," *Anesthesiology*, vol. 119, pp. 507–515, Sept. 2013.

[2] L. Y. Sun and W. S. Beattie, "Association of Intraoperative Hypotension with Acute Kidney Injury after Elective Noncardiac Surgery," *Anesthesiology*, vol. 123, p. 9, Sept. 2015.

[3] World Health Organization, *WHO Guidelines for Safe Surgery*. Geneva: World Health Organization, 2009. OCLC: 901694274.

[4] Committee on Standards and Practice Parameters, "Standards for Basic Anesthetic Monitoring." https://www.asahq.org/standards-and-guidelines/standards-for-basic-anesthetic-monitoring, Oct. 2015.

[5] C. Steiner, Z. Karaca, B. Moore, M. Imshaug, and G. Pickens, "Surgeries in Hospital-Based Ambulatory Surgery and Hospital Inpatient Settings." https://www.hcup-us.ahrq.gov/reports/statbriefs/sb223-Ambulatory-Inpatient-Surgeries-2014.jsp, Feb. 2018.

[6] G. Nuttall, J. Burckhardt, A. Hadley, S. Kane, D. Kor, M. S. Marienau, D. R. Schroeder, K. Handlogten, G. Wilson, and W. C. Oliver, "Surgical and Patient Risk Factors for Severe Arterial Line Complications in Adults," *Anesthesiology*, vol. 124, pp. 590–597, Mar. 2016.

[7] C. Holz and E. J. Wang, "Glabella: Continuously Sensing Blood Pressure Behavior using an Unobtrusive Wearable Device," *Proceedings of the ACM on Interactive, Mobile, Wearable and Ubiquitous Technologies*, vol. 1, pp. 1–23, Sept. 2017.

[8] S. Roth, R. A. Thisted, J. P. Erickson, S. Black, and B. D. Schreider, "Eye Injuries after Nonocular Surgery: A Study of 60,965 Anesthetics from 1988 to 1992," *Anesthesiology*, vol. 85, pp. 1020–1027, Nov. 1996.

[9] W. M. Gild, K. L. Posner, R. A. Caplan, and F. W. Cheney, "Eye Injuries Associated with Anesthesia: A Closed Claims Analysis," *Anesthesiology*, vol. 76, pp. 204–208, Feb. 1992.

[10] Y. Liang, M. Elgendi, Z. Chen, and R. Ward, "An optimal filter for short photoplethysmogram signals," *Scientific Data*, vol. 5, p. 180076, Dec. 2018.